Sn-based Micro and Nano Lithium Battery Materials

T. Clancy, M. Hasan and J.F. Rohan

Tyndall National Institute, University College Cork, Lee Maltings, Cork, Ireland

Energy provision and storage are significant and critical issues for wireless sensor network (WSN) applications. Hybrid energy devices incorporating energy harvesting and storage requires the development of enhanced energy storage materials and architectures. A decreased footprint with the same energy capability is desirable to maximise the energy density and enable long-life wireless sensors. Methods to structure active and support battery materials enhance the device characteristics offering mechanical and electrical support. The results below are for materials that can be processed in 3D or 1D to decrease the footprint of the energy storage element. The effect of the support material is also shown to be significant and directly relevant for high aspect ratio nanostructure where the lithium active materials experience volume changes during charge and discharge.

Introduction

Batteries are the most common energy source for current WSN. However, they exhibit limited capacities and lifetimes that have maintenance schedules measured in months rather than years. The frequent device intervention negates many advantages of wireless sensing. An alternative route to decrease the device intervention frequency is to provide energy that can be replenished daily and to achieve that at reasonable cost and with an appropriate device footprint. Long-life or unlimited wireless sensors for retrofit and energy saving through reduced maintenance requirements are a high priority industry issue, particularly in the commercial buildings arena. Systems with long-life batteries which will not require replacement over a 5-10 years timeframe are highly desirable.

Current energy intensive wireless sensor systems rely on primary (non-rechargeable) batteries. The capacity of the battery is chosen based on the measurement frequency and resulting energy requirements of the WSN. The data in Table 1 shows the capacity required to power a sensor that requires approximately 50 mA pulses for up to 100 ms for data collection and transmission such as for CO_2 sensing. It can be seen that a daily capacity of 1.4 to 2.5 mAh or for 5 years operation between 2 and 5 Ah are required from the energy source, typically batteries, although fuel cells or capacitors are also possible. Capacitors are more appropriate to high power delivery rather than energy storage for long life devices. Typical commercial capacitors exhibit leakage currents that prohibit their use as a standalone energy technology for wireless sensors.

There are many battery chemistries and cell dimensions that can meet the energy requirements at face value. However, a number of other issues must be addressed to achieve an appropriate energy source. Primary batteries, either alkaline or lithium-based are available that can match the capacity requirement for 5 year device lifetime. However, the high current pulse requirements and the associated capacity fade typically result in

significantly less energy availability than that for which the cells are rated. An ideal solution would be sensors with integrated energy harvesting technologies (EHT) and storage. Tthe most common EHT's under investigation are solar, thermal and vibration. Each of these has power densities in the sub mW range, however, sensor operation and data transmission/receipt usually require mA currents for ms timeframes.

TABLE 1. Capacity/Energy required for a WSN delivering 50 mA pulses for 100 ms (and with a standby capacity of 20 mAh required) for a range of sensor operational frequencies. No correction has been included for such issues as self-discharge or other forms of capacity loss over the lifetime of the device.

Measurement Frequency / hr	Capacity/day [mAh]	Capacity/5 years [mAh]	Potential [V]	Energy/5 years [mWh]
Standby only	0.48	876	1.5	1314
1	0.51	937	1.5	1405
4	0.61	1119	1.5	1679
12	0.88	1606	1.5	2409
30	1.48	2701	1.5	4052
60	2.48	4526	1.5	6789

Solar is the most developed energy harvesting technology with the highest power density.

For example

- Commercial Si solar cells can provide < 20 $\mu W/cm^2$ and < 5 $\mu A/cm^2$.
- Dye sensitized solar cells (DSSC) can provide < 100 $\mu W/cm^2$ and < 25 $\mu A/cm^2$.

A research grand challenge is to achieve a 100X improvement in EHT or 10 mW/cm^2 and 2.5 mA/cm^2 in a 7 - 10 year timeframe.

Even with a 100 times improvement it is clear that energy harvesting alone cannot support present day or near future WSNs which can require typical pulse currents of 50 mA. A substantial decrease in the energy requirements for the electronics, sensors and communications is also required for that option to be viable. The intermittent nature of EHT and the low power delivery capability necessitate the integration of appropriate energy storage or power delivery elements in the overall system design. A hybrid device with energy harvesting, storage and high power capability is therefore the optimum solution.

A significant issue for the rechargeable cells is the low current that the harvesting device can deliver to recharge the battery. Matched low capacity cells are better and those that are readily charged at a low rate. Solid state microbatteries have a number of advantages that are appropriate to the WSN energy needs. Thin film microbatteries can deliver 1 mAh capacities in approximately 6 cm^2. A battery of the same dimensions as the solar harvester would be expected to achieve 4.3 mAh meeting the needs of the daily capacity for a hybrid device with EHT and could deliver the tens of mA scale currents required in peak power operation. They exhibit very long lifetimes with 10,000+ cycles possible. They have a stable 4.1V output potential over all of the device lifetime.

There are, however, a number of issues that require development. The batteries are all solid-state and therefore the internal resistance of the cells is significantly larger than for liquid electrolytes. This results in tens of mV drop in potential at high current drain. Large

area 2D cells the same dimension as the solar cells have not been produced to date. A decreased footprint with the same energy capability is also desirable to maximise the energy density and decrease cost. Internationally research investigating methods for 3D and 1D structuring of active and support battery materials to enhance the device characteristics is increasing. (1) Structuring of the support material for enhanced mechanical and electrical characteristics will also assist with nanoscale active materials processing to decrease cost. The results below are for materials that can be processed in 3D or 1D to decrease the footprint of the energy storage element.

Experimental

Cu was sputter deposited on Pyrex wafers and diced into 2 x 1 cm^2 coupons. The substrates were cleaned with acetone and copper oxide removed in a commercial solution (Schloetter S20, sulphuric acid based), rinsed in deionised water and dried with a N_2 gun. An active area of 1 cm^2 was used for deposition. The electrodeposition of Sn was carried out at constant current (0.75 mA cm^{-2}) using a CH Instruments 660C potentiostat in a two electrode arrangement with tin metal as the counter electrode. The Slotolet K bath (Schloetter) was maintained at 20 ± 1^0C for 15 minutes in a quiescent solution. Substrates for Sn deposition were (i) on Cu (200 nm) coated Pyrex, and (ii) 200 nm Ni metallic layer electrodeposited on Cu coated (200 nm) Pyrex. The amount of the Sn deposits and the thickness of the electrodes were measured using a microbalance (Mettler Toledo, XS 105 Dual Range, repeatibility (SD), d = 0.02 mg) and surface profilometer (Tencor alpha-step 200), respectively.

Cu_3Sn_5 nanowire electrodes were prepared from a bath with 0.36 mol dm^{-3} tin methanesulfonate $Sn(O_3SCH_3)_2.4H_2O$, (Sigma Aldrich, 50% wt. as water content) with 0.026 M $Cu(O_3SCH_3)_2.4H_2O$ in 1 M CH_3SO_3H aqueous solution. Additives polyethylene glycol (PEG) (300 ppm) (SigmaUltra, mol. wt. 3350, powder) and Cl^- (50 ppm) as NaCl (BDH, analytical reagent grade) were also added in the electrolyte to suppress the Cu deposition. The deposition was carried out at constant current (5 to 20 mA cm^{-2}) on a Ni substrate at room temperature (20 ± 1 ^{o}C) with moderate stirring. The elemental analysis of the electrodes was by energy dispersive x-ray spectrometry (EDS) (Hitachi S4000 and FEI Nova 630 Nano-SEM coupled with Princeton Gamma technology at 20 KV).

The Li capacity test was performed by cyclic voltammetry and constant current experiments using the CH Instruments 660C potentiostat and a three electrode set-up. The electrolyte consisted of 1M $LiPF_6$ in ethylene carbonate (EC)/diethyl carbonate (DEC) (1:1 by volume) (Sigma-Aldrich). Li foil of 0.25 mm thickness (Sigma-Aldrich) served as counter and reference electrodes. The cell was assembled in an argon-filled glove box (M. Braun Inertgas-System GmbH, Germany) with O_2 and H_2O maintained below 0.1 ppm. The capacity values were measured by calculating the total Coulombic charge during Li^+ ions insertion and extraction for the charge and discharge curves, respectively.

Results and discussion

To achieve an increased energy density per unit footprint it is desirable to utilise materials that can be readily structured in 3D or 1D. In addition it may be necessary to incorporate a core or substrate material also in 3D to mechanically support the active material and to provide electronic conduction pathways for the very high aspect ratio

structures. Typically Cu is utilised as a support material for lithium anodes. We investigated the influence of Cu substrate on Sn which is one of the candidate metal/alloys for high energy density anode materials.

Cyclic voltammograms for thin film (500 nm) Sn electrodes are shown in Fig. 1 (a) on a Cu support and (b) on a Ni support. The cathodic peaks at 1.2-1.6 V, during the early stage of cathodic sweeping are due to the electrolyte reduction as seen with typical graphite electrodes (2-5). The passivation of the Sn electrode due to electrolyte reduction on the first cathodic sweep implies that the electrode is free of the inert Sn oxide layer [10]. The film formation appears for the Ni based electrode only in the first cycle, but for the Sn/Cu electrode it continues for the next few cycles gradually decreasing. This phenomenon originates from the surface roughening during cycling. The large cathodic peaks below 0.4 V are for the main Li^+ ion insertion into the Sn active materials forming $Li_{4.4}Sn$ via multiphase alloys Li_xSn ($2 < x < 4.4$), according to the alloying mechanism (2, 6, 7). The anodic sweep removes Li^+ ion from the $Li_{4.4}Sn$ and produces Li_xSn ($x = 0.7 - 2.33$) alloy phase near 0.75 V, and then, pure metallic Sn near 1.0 V. The peak current decreases rapidly in the Sn/Cu electrode with cycling compared to the buffered Sn/Ni/Cu electrode. The Ni supported Sn exhibits significantly enhanced cycling performance.

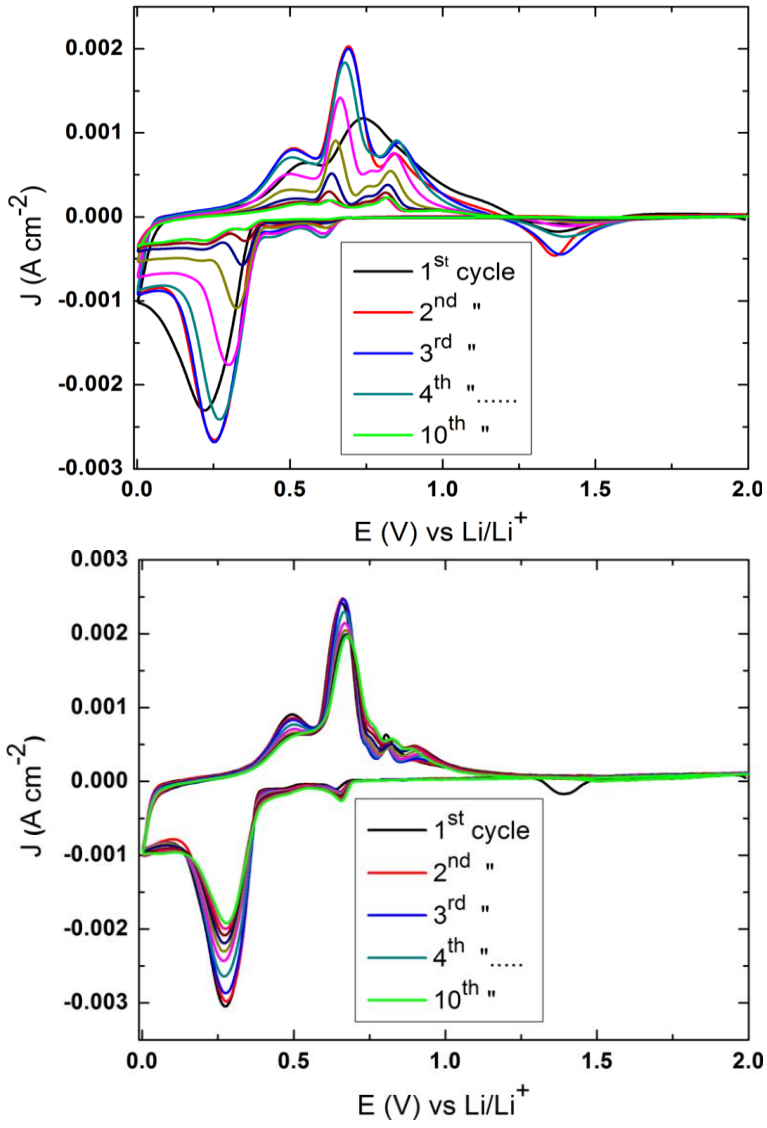

Figure 1. Cyclic voltammograms of Sn thin films (a) Sn/Cu, the inset are peaks for electrolyte reduction and (b) Sn/Ni/Cu electrodes. Sweep rate: 0.5 mV/s.

Fig. 2 (a) shows the charge-discharge capacity vs. cycle number curve of the Sn/Cu electrode. The first cycle shows a charging capacity of 950 $mAhg^{-1}$, which is very close to the theoretical capacity (994 $mAhg^{-1}$). The charging capacity increases slightly from the second (965 $mAhg^{-1}$) to the third cycle (994 $mAhg^{-1}$) and is the maximum capacity of the material. Although, the capacity retention is still 100% in the third cycle, it decreases upon cycling to about 20% after 10 cycles. It also can be seen from Fig. 2 (a) that large irreversible capacity losses (182 $mAhg^{-1}$) in the first cycle may be associated with the formation of the film on the electrode surface. This is due to electrolyte reduction which traps Li^+ ion irreversibly (2, 5, 8).

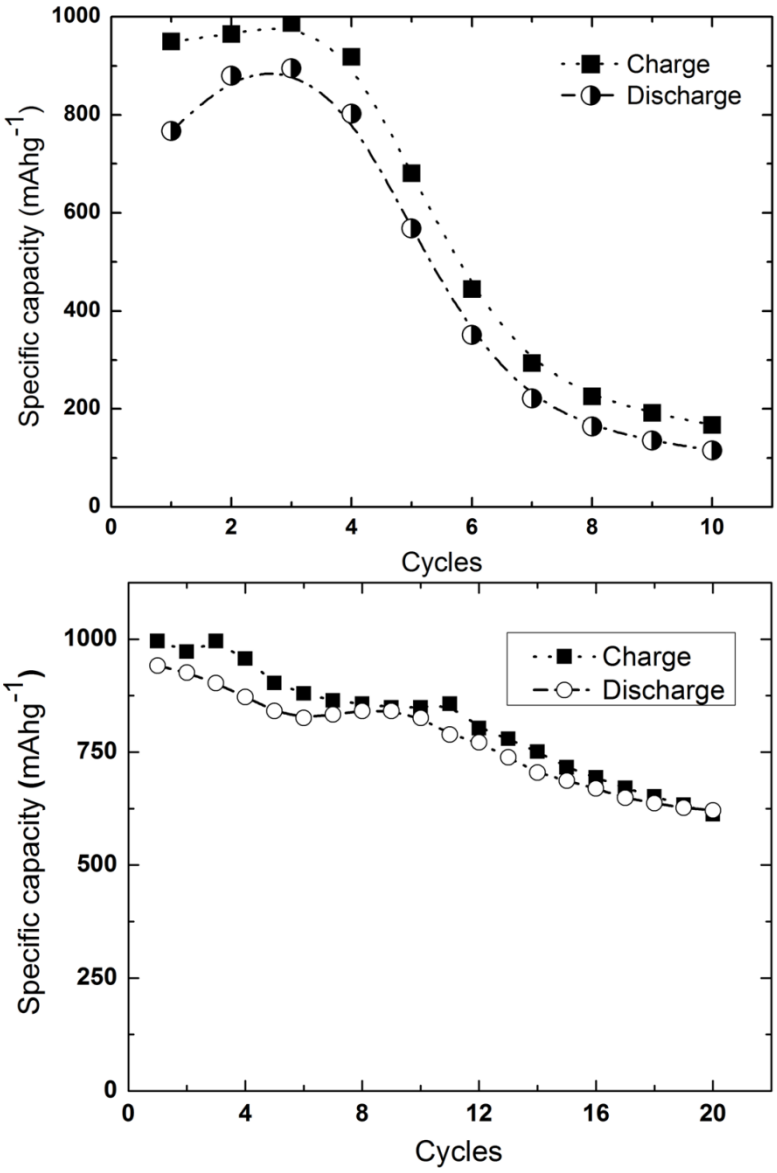

Figure 2. Charge-discharge capacity vs. cycle number curves of (a) Sn/Cu and (b) Sn/Ni electrodes.

At the Ni-Sn interface we consider that there is most likely an intermetallic compound (IMC) of Ni_3Sn_4, which reacts with Li^+ reversibly as suggested by Mukaibo et al. (9, 10). They studied Ni-Sn alloy thin films at different compositions as anode materials, where Ni_3Sn_4 was identified as the main active phase. Therefore, according to the alloying mechanism it is suggested that the reaction of Li^+ ion with Ni_3Sn_4 results in the formation of mixed phases of the disordered Li-Sn alloy and metallic Ni, and the initial IMC layer (Ni_3Sn_4) regenerates in the anodic sweep by absorbing the de-alloyed Sn into a Ni buffering layer. A second IMC layer, Ni-Cu (Li^+ ion inactive) formed at the interface between the Ni buffer layer and the Cu current collector is anticipated to act as a barrier layer against mechanical and electrical integration, and also to act as an adherent layer between the Ni-Sn IMC and the main Cu substrate.

The irreversible capacity loss decreases slightly after the first cycle due to the suppression of electrolyte reduction in the following cycles but still shows a significant amount of irreversible capacity loss of about 50 to 80 $mAhg^{-1}$ (> 5% capacity fade/cycle). This irreversible capacity loss in the continual cycling is attributed to the mechanical disintegration and surface roughening due to volume change during cycling (8, 11). Therefore, a part of the active materials remaining far from the substrate may suffer electrical isolation through lack of interface strength between Sn and Cu which causes irreversible capacity loss.

The charge-discharge capacity variation with cycling of the Ni buffered electrode (Sn/Ni/Cu) for 20 cycles is shown in Fig. 2 (b). The electrode achieved maximum capacity (994 $mAhg^{-1}$) from the beginning and decreases slowly in the continual cycling unlike that seen for the Sn/Cu electrode without the Ni buffering layer. The charging capacities remain at 850 $mAhg^{-1}$ and 612 $mAhg^{-1}$ in the tenth and twentieth cycle, respectively. While the Sn/Cu electrode practically became inactive after 10 cycles, 62% of the total capacity retention is obtained from the Ni buffered Sn/Ni/Cu electrode even after 20 cycles. It is observed in Fig. 4 (b) that a Ni buffer layer also has an effect on very low irreversible capacity loss (54 $mAhg^{-1}$) in the first cycle which is about 3.5 times lower than the Sn/Cu electrode. Although, an irreversible capacity loss slightly increases in the third (90 $mAhg^{-1}$) and the fourth (84 $mAhg^{-1}$) cycle it becomes significantly lower with about < 2% capacity fade from the eighth (15 $mAhg^{-1}$) cycle onwards compared to > 5% capacity fade for Sn/Cu at every cycle following the first.

The electrolyte reduction peak appears only in the first cycle and there are no electrolyte reduction peaks in the following cycles. It appears that the enhanced electrode performance is due to the low irreversible capacity loss and low electrolyte reduction. This indicates that Ni buffering layer improves the cycling performance with respect to electrolyte reduction. However, it does not maintain a constant capacity retention due to the intrinsic crumbling properties and the large volume changes of the Sn during Li^+ ion insertion-de-insertion (6, 12, 13).

Alternative slightly lower capacity materials that can still be processed in 3D were also investigated. We have previously report on the Cu_6Sn_5 anode material and the achievement of a steady capacity after the early cycles (14). The capacity of the Cu_6Sn_5 nanowire anodes stabilized around 200 $mAhg^{-1}$. Higher capacity materials are desirable and a Sn rich Cu alloy was investigated by deposition in an alumina template as described earlier. The composition achieved was Cu_3Sn_5. Cyclic vooltammograms of that material are shown in

figure 3 below. The capacity was 350 $mAhg^{-1}$ initially and decreased to below 300 $mAhg^{-1}$ after only 4 cycles. It appears that Sn rich alloys are not stable as nanowires at least in the absence of a support material in the nanowire. The importance of a conducting and mechanically stable core was shown in our previous work which utilised a Cu core for a lithium active outer copper oxide shell. The nanowire anodes formed maintained a stable capacity over 100 cycles. (15)

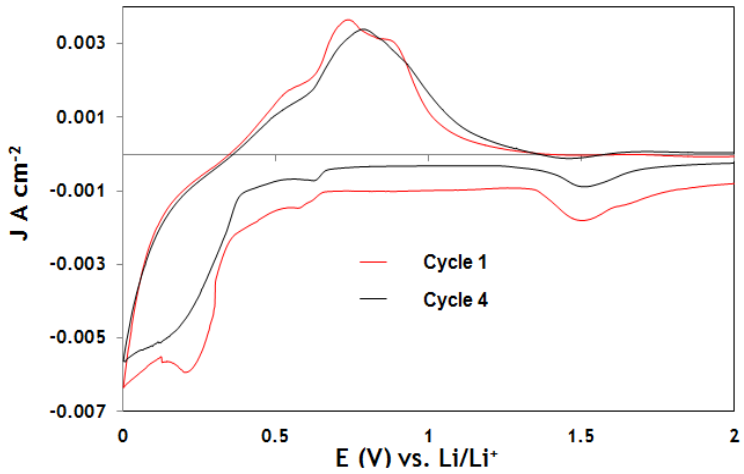

Figure 3. Cyclic voltammograms for Cu_3Sn_5 nanowires Sweep rate: 0.5 mV/s.

Conclusions

Sn thin films were prepared by electrodeposition on Cu and Ni substrates. The Li capacity of Sn thin film electrodes (without a Ni buffering layer) showed very low capacity retention decreasing to about 20% after 10 cycles. The poor capacity retention is associated with the lack of interface strength and irreversible capacity loss is due to passivation of the Sn by the reduction of electrolyte and mechanical disintegration of Sn active materials due to pulverisation. However, an enhanced interface strength is obtained by electroplating a thin layer of Ni between the Sn active material and the Cu substrate. Ni forms two different IMC layers, one at the Sn active material interface and the other one at the Cu current collector interface. The Ni metal present in the first IMC layer at the Sn active material interface buffers the volume changes produced from the Li^+ insertion/de-insertion and consequently results in the decreased pulverisation of the Sn during cycling. Therefore, the extent of electrolyte reduction is low, as no freshly exposed Sn surface is available for the passivation. Finally, the second IMC layer close to the Cu current collector releases the mechanical stress generated during the cycling and keeps the active material electrically contacted. Nanowires of a Sn rich Cu alloy was shown exhibit lithium capacities of around 300 $mAhg^{-1}$ and steady decline in the capacity with cycling. Core-shell nanowire versions incorporating the support which was shown to improve the cycling characteristics of the pure Sn electrodes may be expected to increase the capacity of the high aspect ratio electrodes required to increase the energy density and power delivery capability of microbatteries for future WSN applications.

Acknowledgments

The authors would like to acknowledge support from SFI Grant number 12/IP/1722, Nanomaterials design and fabrication for energy storage.

References

1. J.F. Rohan, M. Hasan, S. Patil, D. Casey and T. Clancy, Chapter 6– *Energy storage materials and architectures at the nanoscale*, in ICT-Energy concepts towards Zero-Power Information and Communication Technology. G. Fagas, L. Gammaitoni, D. Paul and G. Abadal Berini, Editors, p. 107, Intech Publications. (2013)
2. G.V. Zhuang and P.N. Ross, *Electrochem. Solid-St.,* **6,** A136 (2003).
3. K. Xu, *Chem. Rev.*, **104,** 4303 (2004).
4. M. Inaba, H. Tomiyasu, A. Tasaka, S.-K. Jeong and Z. Ogumi, *Langmuir*, **20,** 1348 (2004).
5. L.Y. Beaulieu, S.D. Beattie, T.D. Hatchard and J.R. Dahn, *J. Electrochem. Soc.*, **150**, A419 (2003).
6. M. Winter and J.O. Besenhard, *Electrochim. Acta*, **45**, 31 (1999).
7. I. Rom, M. Wachtler, I. Papst, M. Schmied, J.O. Besenhard, F. Hofer and M. Winter, *Solid State Ionics*, **143**, 329 (2001).
8. M. Inaba, T. Uno and A. Tasaka, *J. Power Sources* **146**, 473 (2005).
9. H. Mukaibo, T. Momma and T. Osaka, *J. Power Sources* **146**, 457 (2005).
10. H. Mukaibo, T. Momma, M. Mohamedi and T. Osaka, *J. Electrochem. Soc.*, **152**, A560 (2005).
11. L.Y. Beaulieu, T.D. Hatchard, A. Bonakdarpour, M.D. Fleischauer and J.R. Dahn, *J. Electrochem. Soc.*, **150**, A1457 (2003).
12. H. Li, L. Shi, Q. Wang, L. Chen and X. Huang, *Solid State Ionics*, **148**, 247 (2002).
13. H. Li, L. Shi, W. Lu, X. Huang and L. Chen, *J. Electrochem. Soc.*, **148**, A915 (2001).
14. J.F. Rohan, M. Hasan and N. Holubowitch, *Electrochim. Acta*, **56**, 9537 (2011),
15. M. Hasan, T. Chowdhury and J.F. Rohan, *J. Electrochem. Soc.*, **157**, A682 (2010).